Chinese Chemical Letters 33 (2022) 394–398

Contents lists available at ScienceDirect

Chinese Chemical Letters

journal homepage: www.elsevier.com/locate/cclet

Low-overpotential electrochemical ammonia synthesis using BiOCl-modified 2D titanium carbide MXene

Yu Wang[a,1], Munkhbayar Batmunkh[b,1], Hui Mao[a,1], Hui Li[a], Baohua Jia[c], Shuyao Wu[a], Daliang Liu[a], Ximing Song[a], Ying Sun[a,*], Tianyi Ma[c,*]

[a] Key Laboratory for Green Synthesis and Preparative Chemistry of Advanced Materials of Liaoning Province, College of Chemistry, Liaoning University, Institute of Clean Energy Chemistry, Shenyang 110036, China
[b] Centre for Catalysis and Clean Energy, School of Environment and Science, Griffith University, Gold Coast, Queensland 4222, Australia
[c] Centre for Translational Atomaterials, School of Science, Swinburne University of Technology, Hawthorn VIC 3122, Australia

ARTICLE INFO

Article history:
Received 24 April 2021
Revised 13 May 2021
Accepted 14 May 2021
Available online 24 May 2021

Keywords:
BiOCl
$Ti_3C_2T_x$
Electrocatalytic
Ammonia
N_2 reduction reaction

ABSTRACT

Electrochemical synthesis of ammonia has the advantages of low energy consumption and promising environmental protection, as compared to the traditional Haber-Bosch process. However, the commercial utilization of this novel system is limited by the low Faradaic efficiency, poor ammonia yield and high overpotential due to the strong N≡N bond and the dominant competing reaction of hydrogen evolution reaction (HER). Herein, a BiOCl-modified two-dimensional (2D) titanium carbide MXenes nanocomposite (BiOCl@$Ti_3C_2T_x$) is proposed as a promising electrocatalyst for ambient nitrogen (N_2) reduction reaction with excellent catalytic performance and superior long-term stability at low overpotential. In 0.1 mol/L HCl, this catalyst attains a high Faradic efficiency of 11.98% and a NH_3 yield of 4.06 μg h^{-1} cm^{-2} at −0.10 V (*vs.* RHE), benefiting from its strong interaction of Bi 6p band with the N 2p orbitals, combined with its large specific surface area and the facile electron transfer.

Ammonia (NH_3) is an important industrial raw material, which has been widely used in agriculture, industry, energy storage and other fields [1–3]. At present, approximately 160 million metric tons of NH_3 is produced by using the traditional Haber-Bosch process, which converts high purity N_2 and H_2 to NH_3 under high temperatures (400–600 °C) and high pressures (200–300 atm), leading to significant energy consumption and CO_2 emissions [4,5]. Therefore, the energy crisis and man-made climate change warn us to explore more sustainable and economical techniques for NH_3 production.

Electrochemical N_2 reduction reaction (NRR) is a promising alternative method that can potentially synthesize NH_3 under ambient conditions [6–8]. However, the robust N≡N bond, the extremely weak N_2 adsorption and the dominant competing reaction of hydrogen evolution reaction (HER) lead to low Faradaic efficiency (FE), unsatisfied ammonia yield and high overpotential, which limit this novel system from its possible commercial utilization [9]. Although substantial progress has been made in this cutting-edge research field, efficient electrocatalysts for NRR are still in demand [10–16]. Bi-based materials, including metal Bi nanoparticles [17], Bi ultrathin nanosheets [18], bismuth oxide [19] and $Bi_4V_2O_{11}/CeO_2$ hybrid [20], exhibit many promising features such as non-toxic, environment-friendly and unique electronic structure [21], endowing them with attractive electrochemical and photocatalytic N_2 reduction potential [22,23]. Studies have shown that the excellent NRR performance of bismuth is attributed to its strong interaction of Bi 6p band with the N 2p orbitals, which facilitates the N_2 adsorption and activation [24,25]. As an important bismuth-based halide, BiOCl has widely been used in photochemistry fields due to its remarkable electrical, optical and catalytic properties, as well as excellent stability [26], but it has been rarely used in electrocatalytic NRR partly due to the inconvenient electrons and protons transformation. Among diversified catalytic performance improvement strategies [27–29], multicomponent strategy is expected to be a simple and effective method, which can enhance the NRR performance of electrocatalysts through reasonable combination of diverse functional components.

In this communication, BiOCl-modified $Ti_3C_2T_x$ MXene (BiOCl@$Ti_3C_2T_x$) was synthesized as a highly efficient electrochemical nitrogen fixation material *via in-situ* hydrothermal growth of BiOCl on the $Ti_3C_2T_x$ (see Supporting information for

* Corresponding authors.
E-mail addresses: yingsun@lnu.edu.cn (Y. Sun), tianyima@swin.edu.au (T. Ma).
[1] These authors contributed equally to this work.

https://doi.org/10.1016/j.cclet.2021.05.025
1001-8417/

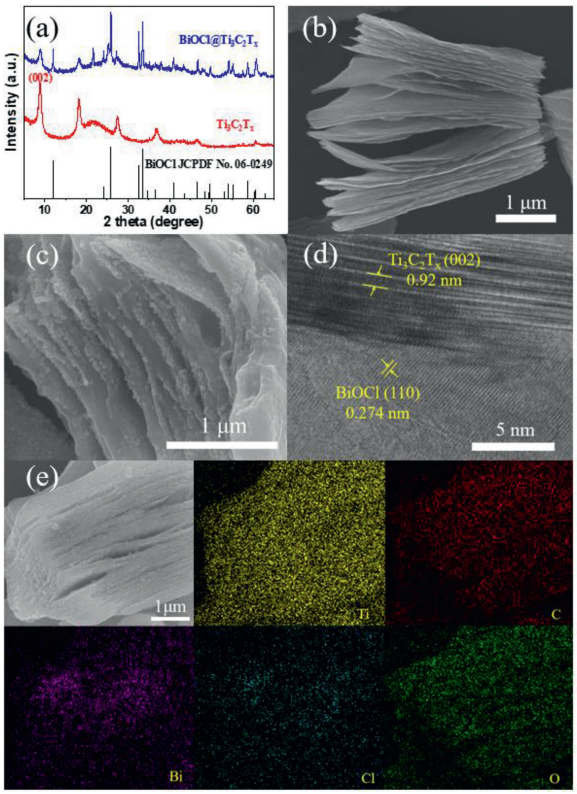

Fig. 1. (a) XRD patterns of BiOCl@$Ti_3C_2T_x$ and $Ti_3C_2T_x$. SEM images of (b) $Ti_3C_2T_x$ and (c) BiOCl@$Ti_3C_2T_x$. (d) HRTEM image of BiOCl@$Ti_3C_2T_x$; (e) EDS elemental mapping images of BiOCl@$Ti_3C_2T_x$.

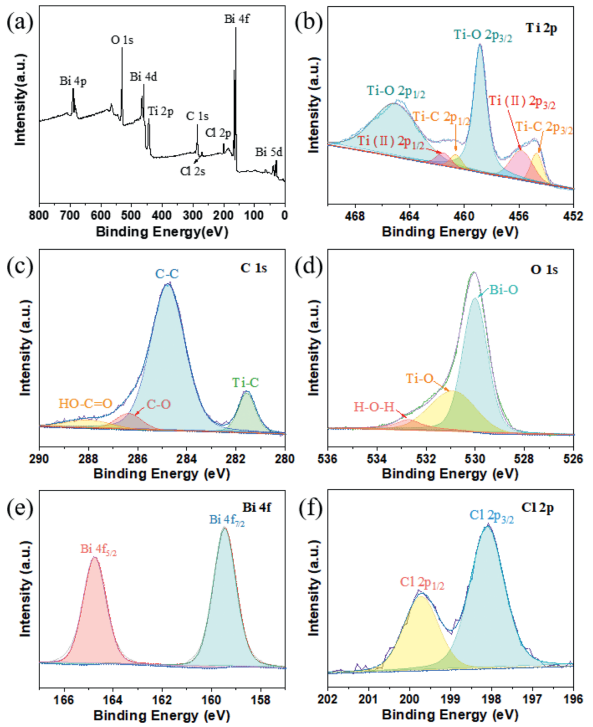

Fig. 2. (a) Survey scan, and (b–f) high-resolution XPS spectra of Ti 2p, C 1s, O 1s, Bi 4f and Cl 2p for BiOCl@$Ti_3C_2T_x$ nanocomposites.

preparation details). The as-obtained BiOCl@$Ti_3C_2T_x$ is superior in NRR activity to its two components under ambient conditions. $Ti_3C_2T_x$, as a new kind of two-dimensional (2D) materials, has been widely used in batteries [30], supercapacitors [31], solar cells [32] and other fields due to its excellent conductivity, stability and large specific surface area [33–36]. As reported, $Ti_3C_2T_x$ also has NRR activity, which could enhance the electron transfer of BiOCl and serve as a robust support to prevent structural changes during electrochemical processes. The NH_3 yield and Faradaic efficiency (FE) of BiOCl@$Ti_3C_2T_x$ at −0.10 V *versus* reversible hydrogen electrode (RHE) were 4.06 μg h^{-1} cm^{-2} and 11.98% in 0.1 mol/L HCl, respectively, which are significantly higher than those obtained by BiOCl (1.05 μg h^{-1} cm^{-2} and 1.88%) and $Ti_3C_2T_x$ (2.26 μg h^{-1} cm^{-2} and 2.43%). Remarkably, this newly designed catalyst also showed good selectivity and electrochemical stability.

The crystalline phase of the obtained BiOCl@$Ti_3C_2T_x$ was studied using an X-ray diffraction (XRD). As shown in Fig. 1a, the characteristic diffraction peak at 9.0° can be assigned to the (002) crystal plane of $Ti_3C_2T_x$ [37], and the peaks appearing at 12.0°, 25.9°, 32.5°, 33.4°, 40.9°, 46.6°, 49.7°, 54.1° and 58.6° are indexed to the (001), (101), (110), (102), (112), (200), (113), (211) and (212) planes of BiOCl (JCPDS No. 06–0249) [38], respectively, indicating the successful preparation of BiOCl@$Ti_3C_2T_x$.

A typical scanning electron microscopy (SEM) image (Fig. 1b) shows the etched $Ti_3C_2T_x$ flakes with a distinct accordion shape and smooth layers separated mostly from each other, indicating the successful removal of Al layer from the Ti_3AlC_2 (MAX) phase. After the hydrothermal reaction, the surface of the as-synthesized BiOCl@$Ti_3C_2T_x$ becomes rough due to the coating of BiOCl nanoparticles as shown in Fig. 1c. The BiOCl nanoparticles, with the particle size of approximately 20 nm, uniformly deposited on the surface of the layered $Ti_3C_2T_x$. This layered structure enables sufficient infiltration of the electrolyte and better exposure of active sites to N_2, and thus yielding a satisfactory electrocatalytic NRR activity. Moreover, the high-resolution transmission electron microscopy (HRTEM) image (Fig. 1d) shows an interplanar spacing of 0.274 nm, indexed to the (110) plane of BiOCl. Furthermore, the energy dispersive X-ray spectroscopy (EDS) elemental mapping analysis of BiOCl@$Ti_3C_2T_x$ further confirms the uniform distribution of Bi, Ti, C, O and Cl elements throughout the catalyst (Fig. 1e). The loading contents of Bi and Ti were 6.47 wt% and 21.78 wt%, respectively, as measured by inductively coupled plasma atomic emission spectrometry (ICP-AES).

X-ray photoelectron spectroscopy (XPS) was employed to study the elemental composition and chemical state of the materials. All binding energies were calibrated against C 1s at 284.8 eV. The survey spectrum of BiOCl@$Ti_3C_2T_x$ composites suggest that the Ti, C, O, Bi and Cl elements exist in the composite (Fig. 2a), which is in excellent agreement with the XRD and EDS mapping. The high-resolution Ti 2p spectrum of BiOCl@$Ti_3C_2T_x$ (Fig. 2b) could be fitted with three doublets (Ti $2p_{3/2}$–Ti $2p_{1/2}$) [39]. The peaks located at 454.7 eV and 455.9 eV correspond to Ti $2p_{3/2}$ binding energies of Ti–C and Ti(II) bond, respectively. The Ti $2p_{1/2}$ of the BiOCl@$Ti_3C_2T_x$ lied in 460.6 eV and 461.5 eV are consistent with the bonds of Ti–C and Ti(II), respectively. While the peaks at 458.9 eV and 465.0 eV correspond to the Ti $2p_{3/2}$ and Ti $2p_{1/2}$ binding energies of the Ti–O bonds, which are due to the presence of abundant hydrophilic functionalities (–O and –OH) after etching by HF [40–42]. In addition, Fig. 2c shows the XPS spectrum of the C 1s region, where the peaks of 281.5, 284.8, 286.4 and 288.1 eV can be associated with the Ti–C, C–C, C–O and HO–C=O bonds, respectively [43–45]. The three peaks at 529.9, 530.9 and 532.6 eV in the O 1s region (Fig. 2d) can be attributed to the Bi–O, Ti–O, and the oxygen containing components (H_2O and –OH) adsorbed on the surface of BiOCl and Ti_3C_2, respectively [46,47]. In Fig. 2e, the peaks at 164.8 and 159.5 eV can be assigned to Bi $4f_{5/2}$ and Bi $4f_{7/2}$, respectively, which can be attributed to Bi^{3+} [43,48]. In

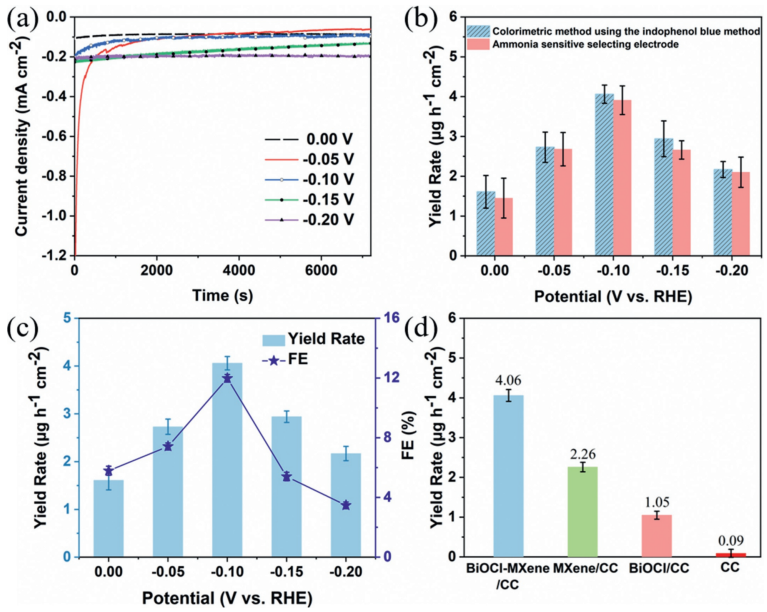

Fig. 3. (a) Time-dependent current density curves at various potentials in N_2-saturated 0.1 mol/L HCl. (b) Comparison of the ammonia-sensitive selecting electrode and indophenol blue reagent-based colorimetric method for the quantitative analysis of ammonia yield. (c) NH_3 yields and FEs of BiOCl@$Ti_3C_2T_x$/CC for the NRR at various potentials. (d) Amount of NH_3 with different electrodes at −0.10 V after 2 h electrolysis under ambient conditions.

Fig. 2f, two peaks at 199.7 and 198.1 eV belong to Cl $2p_{1/2}$ and Cl $2p_{3/2}$, respectively, confirming the existence of Cl^- [49,50]. The SEM, EDS, TEM, ICP-AES and XPS results confirm that the layered 2D composite, BiOCl@$Ti_3C_2T_x$, was successfully prepared.

Electrocatalytic NRR experiments were conducted in a two-compartment electrochemical cell separated by a Nafion membrane (Fig. S2 in Supporting information). The catalysts, BiOCl@$Ti_3C_2T_x$, BiOCl, $Ti_3C_2T_x$, were coated on carbon cloth (CC) (1 cm × 1 cm) (BiOCl@$Ti_3C_2T_x$/CC, BiOCl/CC, $Ti_3C_2T_x$/CC) with a loading of 0.1 mg as the working electrode. The NRR tests were conducted in 0.1 mol/L HCl under ambient conditions. All potentials were reported on the RHE scale. The produced NH_3 were determined by the indophenol blue method [51] and ammonia-sensitive selecting electrode method [52]. The possible by-products (N_2H_4) were tested by the method of Watt and Chrisp [53]. Figs. S3, S4, and S6 (Supporting information) display the calibration curves for the NH_3 concentrations. Fig. S7 (Supporting information) shows the linear sweep voltammetry (LSV) curves for BiOCl@$Ti_3C_2T_x$/CC in Ar- and N_2-saturated 0.1 mol/L HCl solution. It is clearly seen that the BiOCl@$Ti_3C_2T_x$/CC achieved a high current density in N_2-saturated solution, indicating the NRR process on the electrode. A series of potentials from −0.20 V to 0.00 V (*vs.* RHE) were applied to evaluate the NH_3 yields and FEs. Fig. 3a shows the time-dependent current density curves of BiOCl@$Ti_3C_2T_x$/CC at different potentials in N_2-saturated 0.1 mol/L HCl. The ultraviolet-visible (UV-vis) absorption spectra of various electrolytes (Fig. S8 in Supporting information) indicates that the NRR is produced at various potentials. In addition, the concentrations of the NH_3 were also determined by ammonia-sensitive selecting electrode method to confirm the reliability of colorimetric method. As shown in Fig. 3b, the NH_3 yields are very close to those obtained by indophenol blue method, indicating that it is reliable to use the indophenol blue method for the quantitative analysis of the produced NH_3.

The NH_3 yields and FEs of the BiOCl@$Ti_3C_2T_x$/CC at various potentials are calculated and have been summarized in Fig. 3c. As observed, the maximum values of NH_3 yield and FE were determined to be 4.06 μg h^{-1} cm^{-2} and 11.98% at −0.10 V (*vs.* RHE), respectively. This NRR catalytic performance of the as-prepared BiOCl@$Ti_3C_2T_x$ nanocomposite can even be comparable to the yields achieved by some metal-MXene hybrid nanocatalysts at higher overpotential (*e.g.*, Ru@MXene (NH_3 yield rate of 2.3 μmol h^{-1} cm^{-2} at −0.4 V (*vs.* RHE) in 0.1 mol/L KOH electrolyte) [54], Mo_2C/C (NH_3 yield rate of 11.3 μg h^{-1} mg^{-1} at −0.3 V (*vs.* RHE) in 0.5 M Li_2SO_4 electrolyte) [55] and $Ti_3C_2T_x$/FeOOH (NH_3 yield rate of 0.53 μg h^{-1} cm^{-2} at −0.5 V (*vs.* RHE) in 0.5 mol/L Li_2SO_4 electrolyte) [56]). In addition, it should be noted that this work realized the high efficiency ammonia production catalyzed by bismuth-based materials at a low potential of −0.1 V for the first time. It can be observed that when the applied potential becomes more negative, the NH_3 yield and FE decrease owing to the competitive HER [57,58]. Notably, the by-product N_2H_4 was hardly detected (Fig. S9 in Supporting information), indicating that the BiOCl@$Ti_3C_2T_x$ possessed excellent selectivity toward NH_3 production. We further quantified the amount of NH_3 produced on blank CC, BiOCl/CC, $Ti_3C_2T_x$/CC and BiOCl@$Ti_3C_2T_x$/CC to verify the activity of BiOCl@$Ti_3C_2T_x$. As shown in Fig. 3d, the bare CC has necessitous electrocatalytic NRR activity, while the BiOCl/CC and $Ti_3C_2T_x$/CC are active for the NRR, producing 1.05 and 2.26 μg h^{-1} cm^{-2} of NH_3, respectively. Indeed, the BiOCl@$Ti_3C_2T_x$/CC exhibited greatly enhanced electrocatalytic NRR activity producing 8.12 μg h^{-1} cm^{-2} of NH_3, which is about 3.9 times higher than that of BiOCl/CC and 1.8 times greater than that of $Ti_3C_2T_x$/CC, suggesting that both BiOCl and $Ti_3C_2T_x$ work synergistically to catalyze the N_2 fixation.

The superior NRR activity of BiOCl@$Ti_3C_2T_x$ nanocomposites is attributed to the following points: (1) MXene as an ideal support owing to its large specific surface area can fully load BiOCl and avoid aggregation of BiOCl, thus exposing more active sites; (2) The strong interaction between the Bi 6p band of semiconducting BiOCl and the N 2p orbitals can effectively restrain the HER activity of $Ti_3C_2T_x$, and thereby achieving high FEs; (3) The double-layer capacitance measurement demonstrates that the BiOCl@$Ti_3C_2T_x$ possesses a much larger capacitance and thus exposes more electrochemically active surface area (Fig. S10 in Supporting information). Finally, $Ti_3C_2T_x$ substrate has an excellent electrical conductivity

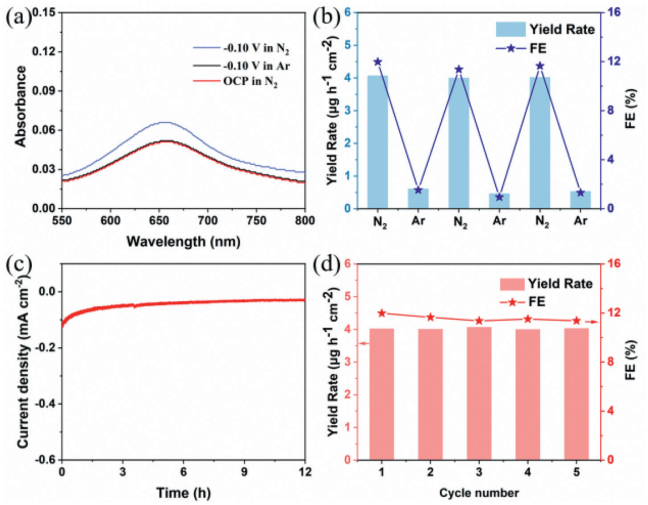

Fig. 4. (a) UV-vis absorption spectra of the electrolytes stained with the indophenol indicator after NRR electrolysis using BiOCl@$Ti_3C_2T_x$/CC for 2 h under different conditions. (b) NH_3 yields and FEs for BiOCl@$Ti_3C_2T_x$/CC with alternating 2 h cycles between Ar- and N_2-saturated electrolytes. (c) Time-dependent current density curve for the BiOCl@$Ti_3C_2T_x$ catalyst at −0.10 V for 12 h. (d) Recycling stability tests on BiOCl@$Ti_3C_2T_x$/CC at −0.10 V for 5 times.

favoring for rapid electron transport in the NRR process, resulting in a higher NH_3 yield rate.

To confirm that the produced NH_3 was generated *via* NRR, we executed control experiments in an Ar- and N_2-saturated solution at −0.10 V for 2 h, as well as in N_2-saturated solution at open circuit potential for 2 h, respectively. The UV-vis absorption spectra show that the NH_3 was produced only in the N_2-saturated solution (Fig. 4a). We also carried out 12 h cycling test with an interval of 2 h in N_2- and Ar-saturated solution at −0.10 V (Fig. 4b). Fig. 4b further confirms that the produced NH_3 primarily generated from the catalysis of N_2. The durability and stability are also crucial indicator to estimate the performance of electrocatalysts. As shown in Fig. 4c, the current density shows no obvious difference during 12 h catalysis at −0.10 V. During cycling test over five times, both the NH_3 yield and FE show negligible change (Fig. 4d). Both the compositions and BiOCl nature of the BiOCl@$Ti_3C_2T_x$ could be well maintained after the long-term electrocatalysis reaction when comparing SEM, TEM (Fig. S11 in Supporting information) and XPS images (Fig. S12 in Supporting information) before and after the reaction, demonstrating the excellent electrochemical durability of the BiOCl@$Ti_3C_2T_x$ for the NRR, which is another crucial factor for the enhancement of NRR performances.

In conclusion, BiOCl-modified $Ti_3C_2T_x$ MXene is used as an efficient electrocatalyst for N_2-to-NH_3 with a high FE at a low overpotential. In 0.1 mol/L HCl, the BiOCl@$Ti_3C_2T_x$ nanocomposite can achieve a NH_3 yield rate of 4.06 μg h^{-1} cm^{-2} with FEs of 11.98% at −0.10 V *vs.* RHE. Meanwhile, BiOCl@$Ti_3C_2T_x$ shows superior stability and high selectivity. The high performance of the obtained BiOCl@$Ti_3C_2T_x$ toward NRR could be ascribed to the sufficient exposure of active catalytic sites of Bi and Ti, the inhibition of HER by Bi. Both BiOCl and $Ti_3C_2T_x$ synergistically enhance the NRR performance. This study provides a new avenue for the development and design of Bi-based catalysts as advanced electrocatalysts for artificial N_2 reduction.

Declaration of competing interest

The authors declare that they have no known competing financial interests or personal relationships that could have appeared to influence the work reported in this paper.

Acknowledgments

This work was supported by the National Natural Science Foundation of China (No. 52071171), the Liaoning Revitalization Talents Program - Pan Deng Scholars (No. XLYC1802005), the Liaoning BaiQianWan Talents Program (No. LNBQW2018B0048), Natural Science Fund of Liaoning Province for Excellent Young Scholars (No. 2019-YQ-04), the Key Project of Scientific Research of the Education Department of Liaoning Province (No. LZD201902), the Young Scientific and Technological Talents Project of the Department of Education of Liaoning Province (Nos. LQN201903 and LQN202008), the Foundation for Young Scholars of Liaoning University (No. LDQN2019007).

Supplementary materials

Supplementary material associated with this article can be found, in the online version, at doi:10.1016/j.cclet.2021.05.025.

References

[1] H.K. Lee, C.S.L. Koh, Y.H. Lee, et al., Sci. Adv. 4 (2018) eaar3208.
[2] B.M. Hoffman, D. Lukoyanov, Z.Y. Yang, et al., Chem. Rev. 114 (2014) 4041–4062.
[3] I. Coric, B.Q. Mercado, E. Bill, et al., Nature 526 (2015) 96–99.
[4] C.J.M. van der Ham, M.T. Koper, D.G. Hetterscheid, Chem. Soc. Rev. 43 (2014) 5183–5191.
[5] M. Kitano, Y. Inoue, Y. Yamazaki, et al., Nat. Chem. 4 (2012) 934–940.
[6] Y. Yao, S. Zhu, H. Wang, et al., J. Am. Chem. Soc. 140 (2018) 1496–1501.
[7] D. Bao, Q. Zhang, F.L. Meng, et al., Adv. Mater. 29 (2017) 1604799.
[8] M. Bat-Erdene, G. Xu, M. Batmunkh, et al., J. Mater. Chem. A 8 (2020) 4735–4739.
[9] G.F. Chen, X. Cao, S. Wu, et al., J. Am. Chem. Soc. 139 (2017) 9771–9774.
[10] G.F. Chen, S. Ren, L. Zhang, et al., Small Methods 3 (2018) 1800337.
[11] Y. Sun, Y. Wang, H. Li, et al., J. Energy Chem. 62 (2021) 51–70.
[12] G. Xu, H. Li, A.S.R. Bati, et al., J. Mater. Chem. A 8 (2020) 15875–15883.
[13] T. Wang, Q. Liu, T. Li, et al., J. Mater. Chem. A 9 (2021) 884–888.
[14] T. Wang, S. Li, B. He, et al., J. Catal. 42 (2021) 1024–1029.
[15] S. Li, Y. Wang, J. Liang, et al., Mater. Today Phys. 18 (2021) 100396.
[16] F. Wang, L. Mao, H. Xie, et al., Small Struct. 2 (2021) 2000075.
[17] D. Yao, C. Tang, L. Li, et al., Adv. Energy Mater. 10 (2020) 2001289.
[18] Y. Xu, T. Ren, S. Yu, et al., Sustain. Energy Fuels 4 (2020) 3334–3339.
[19] B. Chang, Q. Liu, N. Chen, et al., ChemCatChem 11 (2019) 1884–1888.
[20] C. Lv, C. Yan, G. Chen, et al., Angew. Chem. Int. Ed. 57 (2018) 6073–6076.
[21] M. Huang, B. Xi, N. Shi, et al., Small Struct. 2 (2021) 2000085.
[22] L. Li, C. Tang, B. Xia, et al., ACS Catal. 9 (2019) 2902–2908.
[23] Y. Bi, Y. Wang, X. Dong, et al., RSC Adv 8 (2018) 21871–21878.
[24] Y.C. Hao, Y. Guo, L.W. Chen, et al., Nat. Catal. 2 (2019) 448–456.
[25] Y. Sun, Z. Deng, X.M. Song, et al., Nanomicro. Lett. 12 (2020) 133.
[26] P. M. Jahani, H. A. Javar, H. Mahmoudi-Moghaddam, J. Mater. Sci. Mater. El. 31 (2020) 14022–14034.
[27] Y. Fu, P. Richardson, K. Li, et al., Nanomicro. Lett. 12 (2020) 65–77.
[28] T Xu, B Ma, J Liang, et al., Acta Phys. -Chim. Sin. 37 (2021) 2009043.
[29] B. Ma, H. Zhao, T. Li, et al., Nano Res. 14 (2020) 555–569.
[30] C. Chen, X. Xie, B. Anasori, et al., Angew. Chem. Int. Ed. 57 (2018) 1846–1850.
[31] C. Zhang, L. McKeon, M.P. Kremer, et al., Nat. Commun. 10 (2019) 1795.
[32] L. Yu, A.S.R. Bati, T.S.L. Grace, et al., Adv. Energy Mater. 9 (2019) 1901063.
[33] X. Hui, X. Ge, R. Zhao, et al., Adv. Funct. Mater. 30 (2020) 2005190.
[34] A. Liu, X. Liang, X. Ren, et al., Adv. Funct. Mater. 30 (2020) 2003437.
[35] R.A. Soomro, S. Jawaid, Q. Zhu, et al., Chin. Chem. Lett. 31 (2020) 922–930.
[36] J. Tan, S. Li, B. Liu, et al., Small Struct. 2 (2021) 2000093.
[37] T. Li, X. Yan, L. Huang, et al., J. Mater. Chem. A 7 (2019) 14462–14465.
[38] W. Hou, C. Deng, H. Xu, et al., ChemistrySelect 5 (2020) 2767–2777.
[39] R. Zhao, H. Di, X. Hui, et al., Energ. Environ. Sci. 13 (2020) 246–257.
[40] J. Xia, S.Z. Yang, B. Wang, et al., Nano Energy 72 (2020) 104681.
[41] J. Zhang, M. Liu, Y. Wang, et al., CrystEngComm 22 (2020) 3683–3691.
[42] X. Lu, Q. Zhang, J. Liao, et al., Adv. Energy Mater. 10 (2019) 1902986.
[43] S. Cao, B. Shen, T. Tong, et al., Adv. Funct. Mater. 28 (2018) 1800136.
[44] H. Chen, G. Ke, X. Wu, et al., Chem. Eng. J. 406 (2021) 126775.
[45] Q. Liu, L. Ai, J. Jiang, J. Mater. Chem. A 6 (2018) 4102–4110.
[46] Q. Xi, X. Yue, J. Feng, et al., J. Solid State Chem. 289 (2020) 121470.
[47] S. Wu, Y. Su, Y. Zhu, et al., Appl. Surf. Sci. 520 (2020) 146339.
[48] Y. Chen, F. Wang, Y. Cao, et al., ACS Appl. Energy Mater. 3 (2020) 4610–4618.
[49] W. He, Y. Wang, C. Fan, et al., RSC Adv. 9 (2019) 14286–14295.
[50] Y. Cai, D. Li, J. Sun, et al., Appl. Surf. Sci. 439 (2018) 697–704.
[51] D. Zhu, L. Zhang, R.E. Ruther, et al., Nat. Mater. 12 (2013) 836–841.
[52] B. Yu, H. Li, J. White, et al., Adv. Funct. Mater. 30 (2019) 1905665.

[53] G.W. Watt, J.D. Chrisp, Anal. Chem. 24 (1952) 2006–2008.
[54] A. Liu, M. Gao, X. Ren, et al., Nanoscale 12 (2020) 10933–10938.
[55] H. Cheng, L.X. Ding, G.F. Chen, et al., Adv. Mater. 30 (2018) e1803694.
[56] Y. Luo, G.F. Chen, L. Ding, et al., Joule 3 (2019) 279–289.
[57] X. Ren, J. Zhao, Q. Wei, et al., ACS Cent. Sci. 5 (2019) 116–121.
[58] W. Qiu, X.Y. Xie, J. Qiu, et al., Nat. Commun. 9 (2018) 3485.